CHAPTER 3

BEAM-WAVE INTERACTION ANALYSIS OF AN AXIALLY PERIODIC DISK-LOADED SLOW-WAVE STRUCTURE WITH LOW-LOSS DIELECTRIC FILLING BETWEEN DISKS FOR A MAGNETICALLY INSULATED LINE OSCILLATOR (MILO)

3.1 Outline

The partially dielectric-infused axially periodic disk-loaded co-axial SWS was analyzed in the presence of beam like an interaction structure for MILO. The electron beam present region (i.e. Region -I) was analyzed by the use of Maxwell's fluid equation in linear form (i.e. Vlasov-Maxwell's equation). The less –loss dielectric medium is partly filled in the slow wave structure (SWS), which is made of periodical disk- loaded coaxial structure. The dispersion relationship and temporal growth rate have been found out by considering all the harmonics created in the structure. The influence of dielectric material on various parameters (i.e. dispersion characteristics, interaction impedance, phase velocity etc.) has already been discussed in beam absent analysis of partially DFMILO. To verify the completed theoretical study, the analytically generated dispersion values were compared with previously recorded dispersion findings. The commercial software "Computer Simulation Tool (CST) Studio Suite" was also used to corroborate the results." The results were compared to previously published literature, and show good agreement of simulated and theoretical results with less than 5%.

3.2 Introduction

The magnetically insulated transmission line oscillator is important and the most popular among HPM devices due to its small size and capacity to produce high- peak radio frequency (RF) power in multiple gigawatt ranges. The main attractive feature of MILO is no requirement of an external DC magnetic field by which problem of electric breakdown, does not occur. The MILO device is based on intense relativistic electron beam (IREB) followed by relativistic Brillouin flow (RBF) [Dwivedi and Jain, 2012]. MILO is the extension of a linear Magnetron. For the purpose of operating MILO, a DC pulse voltage of high magnitude is provided between the anode and cathode sections. Due

to which explosive emission takes place from the cylindrical cathode surface, as a result high – intensity relativistic electrons get released from the cylindrical cathode surface [Benford *et al.,* 2007]. In a device, generation of load current depends upon the relativistic electrons emitted from the cathode and these electrons move towards the anode radially. Load current is responsible for providing the magnetic insulation in the device when its value exceeds the critical current [Lemke *et al.,* 1987].

The electron beam is guided by the device due to properties of self – magnetic insulation property without the need of an external DC – magnetic field. It can function at huge voltages without vacuum breakdown because only one source is required for the operation of the device. MILO has several attractive features, but it has some drawbacks like low conversion efficiency and pulse shorting. The main challenges of the researchers are to overcome the pulse shorting issue and to enhance the conversion efficacy of the device [Kumar *et al*., 2020]. The researchers continue modifying the structural design, modifying types of the cylindrical cathode section, different types of anode section, because they are responsible for RF interaction in the device, the output section etc. for improving the efficiency of the device by which RF output power is increases and to overcome the pulse shorting problem.

There are numerous literature reported investigating the beam-wave interaction structure using various techniques; for example, Lemke et al. combined linear theory and the thin beam approximation for a coaxial structure with a square wave type periodic anode, but the important restriction associated with their examination is that it is applicable to only symmetric TM_{0n} mode [Lemke *et al*., 1987]. Zhang et al. evaluated a periodic disc-loaded cylindrical waveguide construction with axial and azimuthal corrugations by making use of a modified Rayleigh-Fourier approach electron beam [Haworth *et al.,* 1998]. Sagor *et al*. employed a linear analysis for a circular-edge disk-

loaded cylindrical waveguide structure operated by an annular electron beam [Sagor and Amin 2017]. Dwivedi *et al.* employed a modal matching approach to discover the temporal growth rate of the symmetric TM_{01} mode for a disc loaded coaxial structure around the vicinity of an electron beam [Dwivedi and Jain 2012].

One novel method to raise the efficiency of the device is dielectric loading in the SWS structure which increases the effective capacitance of the structure. Dielectric loading in the structure gives another controlling tool for the dispersion curve, increased RF out- put, improved RF spectrum and also imparts frequency tunability by altering the dielectric thickness or dielectric materials. Dielectric loading is a concept that has previously been employed in a number of microwave tubes like gyrotron travelling wave tube (gyro-TWT), gyro-twystron, magnetron, and MILO [Lemke *et al.,* 1987, Zhang *et al.,* 2005, Sagor and Amin, 2017 and Dwivedi and Jain, 2012]. More opportunities for enhancing device conversion efficiency and frequency tuning are made available by the idea of dielectric loading in a device. So, the partially dielectric filled periodic disk – loaded co- axial SWS MILO being investigated in the presence of an electron beam. There are various ways to investigate the slow wave properties of any interaction structure, including field matching, mode matching, and equivalent circuit analysis.

The field matching method is used in this article to analyze the partially dielectric filled periodic disk – loaded co- axial SWS in electron beam presence, extending the theory from the beam absent case (cold analysis). This analysis is used to explain dispersion curve when electron beam is present and also the temporal growth rate of the device. The effect of dielectric loading on phase velocity, interaction impedance and dependency on structural parameters has already been discussed in the beam absent analysis of the device [Upadhyay *et al.,* 2022]. Furthermore, using a field matching approach, one can derive the dispersion characteristics for any symmetric TM mode that

cannot be achieved by equivalent circuit analysis Fan et al [Fan *et al.,* 2015]. The relevant electromagnetic (EM) field expressions in various regions of structure, boundary conditions, and the final expression of the dispersion relationship and temporal growth rate for the symmetric TM mode are all deduced in Section II. Section III provides a detailed explanation of the results of the analytical approach and simulation tool, respectively. Finally, in Section IV, the work is summarized.

3.3 Analytical approach

In MILO, the periodic metal disk-loaded co-axial structure is a popular RF interaction structure. The low-loss dielectric material having fixed thickness is partially fitted in the middle of successive metal discs to enhance the beam–wave interaction. Only the real component of the dielectric constant (i.e.,ε_r) is examined in the analysis, and the imaginary portion of the dielectric constant is assumed to be little. As a result, the dielectric material's loss tangent has a very low value, and the influence of loss tangent may be disregarded. Experimentally, the impact of a low-loss dielectric material is discussed in [Zhang *et al.,* 2012], which employed a very low-loss dielectric material with a very low loss tangent value. The dielectric loading inside the interaction cavity helps in raising the efficacious capacitance of the cavity that increases the cavity's capacity for storing energy. This RF energy is initially held as a standing wave, which the extractor cavity subsequently couples out to create a travelling wave. Figure 3.1 shows an illustration of a partially dielectric-filled periodic disk-loaded co-axial structure when the electron beam is present. The partially dielectric-filled periodic disk-loaded co-axial structure with an electron beam is depicted in section Fig. 3.1(a), its unit cell is presented in Fig. 3.1(b) and the front view is depicted in Fig. 3.1(c). The cylindrical coordinate system (r,θ,z) is used for present analysis.

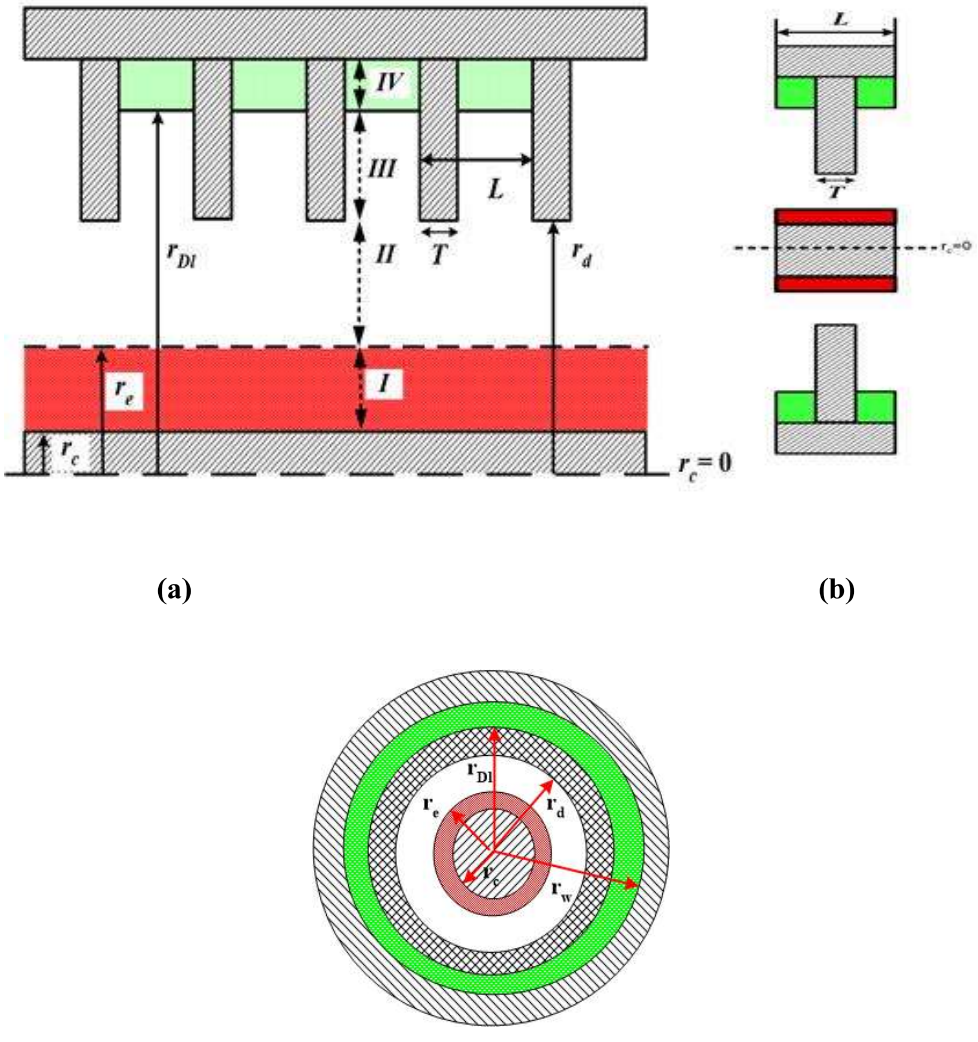

(a) **(b)**

(c)

Figure 3.1: Schematic of a partially dielectric filled axially periodic metal disc loaded coaxial structure with beam-present in red colour: **(a)** sectional view, **(b)** unit cell **(c)** Front View

The device's analysis of the beam-wave interaction primarily emphasizes finding the dispersion relation (in electron beam analysis) along with temporal growth rate. The dispersion relation along with the temporal growth rate is determined on the premise that in region-I, a parapotential flow equilibrium forms which causes the creation of space-charge waves [Zhang *et al.,* 2005]. The space charge wave mostly participates in beam-

wave interaction and produces RF in the vicinity of the anode section (near the tip of the periodically loaded disc (r_d)). Further assumption is made that the region-II aids the travelling wave that gets effected by the space charge wave developed in region-I .The whole structure is categorized in four regions; region-I (i.e. electron beam present region ($r_c < r < r_e$)), region-II [i.e., disk-free region ($r_c < r < r_d$)], region-III [i.e., disk occupied region ($r_d < r < r_{Dl}$)], and region-IV [i.e., partially dielectric-filled region ($r_{Dl} < r < r_w$)]. L is the axial periodicity, T is the thickness of the disk, r_e is the electron beam radius, r_c is the radius of the cylindrical cathode, r_d is the disk hole radius, and r_w is the inner wall radius of the outer conductor as shown in Fig. 3.1(a). According to Floquet theorem, if a device have axial periodicity, then the unit cell (depicted in Fig. 3.1 (b)) of the device is adequate for analysis. This structure is analyzed for TM modes ($H_z = 0$) using the field matching approach. The EM fields are assumed to be time-independent and that region-I and region – II, have travelling waves although region-III and region – IV have standing waves before the structure is analyzed. The travelling wave's space harmonics are caused by the structure's axial periodicity, but the standing wave's modal harmonics are caused by reflections off its metallic surfaces. Regions I through IV's related parameters are denoted by superscripts I and IV, respectively.

3.3.1 EM Field Expression for Region-I (i.e., $r_c < r < r_e$)

Region–I defines the coaxial cylindrical cathode and the outer radius of the electron beam. For analysis of the electron beam region linear Maxwell (i.e. Vlasov-Maxwell's equation) is used [Dwivedi *et al., 2012 and* R.W. Lemke *1989*]:

$$\left(\frac{\partial}{\partial t}+v_z\frac{\partial}{\partial z}\right)P_z=-eE_z \tag{3.1}$$

$$\frac{1}{r}\frac{\partial}{\partial r}\left(rE_r\right)+\frac{\partial E_z}{\partial z}=-4\pi en_e \tag{3.2}$$

$$\frac{\partial E_r}{\partial z} - \frac{\partial E_z}{\partial r} = -\frac{1}{c}\frac{\partial B_\theta}{\partial t} \tag{3.3}$$

$$-\frac{\partial B_\theta}{\partial z} = \frac{1}{c}\frac{\partial E_r}{\partial t} \tag{3.4}$$

$$\frac{1}{r}\frac{\partial (rB_\theta)}{\partial z} = \frac{4\pi}{c}J_z + \frac{1}{c}\frac{\partial E_z}{\partial t} \tag{3.5}$$

$$\left(\frac{1}{r}\frac{d}{dr}r\frac{d}{dr} + \gamma_n^2\right)E_{z,n} = \frac{\alpha c^2}{(\pi/2)r_e}\frac{\gamma_n^2 E_{z,n}}{(\omega - v_z\beta_n)^2}\delta(r - r_e) \tag{3.6}$$

Here $\gamma = 1/(1 - v_z^2/c^2)^{1/2}$ is the relativistic factor, $P_z = \gamma m v_z$ is axial momentum $J_z = -\eta e n_e v_z \delta(r - r_e)$ is the axial current density , n_e is the charge number density , $\delta(r - r_e)$ is delta function, v_z is the axial drift velocity, and r_e is electron beam radius. The parameter η is normalized factor evaluated by, $\eta = |I_e|/(2\pi e r_e n v_z)$. The electric and magnetic field components for TM modes are obtained by solving the preceding equation as follows:

$$E_{r,n} = i\frac{\beta_n}{\gamma_n^2}\frac{dE_{z,n}}{dr} \tag{3.7}$$

$$B_{\theta,n} = i\frac{\omega/c}{\gamma_n^2}\frac{dE_{z,n}}{dr} \tag{3.8}$$

$$\left(\frac{1}{r}\frac{d}{dr}r\frac{d}{dr} + \gamma_n^2\right)E_{z,n} = \frac{\alpha c^2}{(\pi/2)r_e}\frac{\gamma_n^2 E_{z,n}}{(\omega - v_z\beta_n)^2}\delta(r - r_e) \tag{3.9}$$

Here, $\gamma_n^2 = \omega^2/c^2 - \beta_n^2$ is the radial propagation constant, and $\alpha = \pi|I_e|/(\gamma_n^2 I_A)$ with $I_A = 17.1\gamma v_z/c$ kA is the Alfven current. With help of calculation of axial electric (E_z) and axial magnetic field (H_z), the four transverse field components is evaluated using Maxwell's equation as:

$$E_r^{\Re} = \left(\frac{-j}{\gamma_n^2}\right)\left\{\beta_n \frac{\partial E_z^{\Re}}{\partial r} + \frac{\omega\mu}{r}\frac{\partial H_z^{\Re}}{\partial \theta}\right\} \tag{3.10}$$

$$E_\theta^{\Re} = \left(\frac{-j}{\gamma_n^2}\right)\left\{\frac{\beta_n}{r}\frac{\partial E_z^{\Re}}{\partial \theta} - \omega\mu\frac{\partial H_z^{\Re}}{\partial r}\right\} \tag{3.11}$$

$$H_r^{\Re} = \left(\frac{j}{\gamma_n^2}\right)\left\{\frac{\omega\varepsilon}{r}\frac{\partial E_z^{\Re}}{\partial \theta} - \beta_n\frac{\partial H_z^{\Re}}{\partial r}\right\} \tag{3.12}$$

$$H_\theta^{\Re} = \left(\frac{-j}{\gamma_n^2}\right)\left\{\omega\varepsilon\frac{\partial E_z^{\Re}}{\partial r} - \frac{\beta_n}{r}\frac{\partial H_z^{\Re}}{\partial \theta}\right\} \tag{3.13}$$

Here, superscript $\Re$ stand for region-*I*, *II*, *III* and *IV* for corresponding regions. The structure employed in the present investigation is azimuthally symmetric, and thus $(\partial/\partial\theta) = 0$. Region – I contains electron beam for the RF interaction. The Region-*I* is considered to have all the space harmonics since it has a travelling RF beam. The electron mobility is radially constant in this area, hence there is no energy source in this region. For region I, the appropriate beam present field expression is as follows:

$$H_z^I = 0 \tag{3.14}$$

$$E_\theta^I = 0 \tag{3.15}$$

$$H_r^I = 0 \tag{3.16}$$

$$E_Z^I = \sum_{n=-\infty}^{\infty} J_0\left(G_{2,n}r\right)A_n^I e^{-j\beta_n^I Z} \tag{3.17}$$

$$E_r^I = \sum_{n=-\infty}^{\infty} \frac{-j\beta_n^I G_{2,n}}{\left(\gamma_n^I\right)^2} J_1\left(G_{2,n}r\right)A_n^I e^{-j\beta_n^I Z} \tag{3.18}$$

$$H_\theta^I = \sum_{n=-\infty}^{\infty} \frac{-j\omega\varepsilon G_{2,n}}{\left(\gamma_n^I\right)^2} J_1\left(G_{2,n}r\right)A_n^I e^{-j\beta_n^I Z} \tag{3.19}$$

Here, $\beta_n = \beta_0 + 2n\pi / L$ is the axial propagation constant; $G_{2,n} = \left(\frac{\Gamma_n^* \gamma}{\varsigma}\right)^2 - \frac{1}{3}$,

$\Gamma_n^* = \frac{\gamma_n}{\sqrt{1 - \frac{\omega_p^2}{\gamma_0^3 \Omega_n^2}}}$, $\omega_p = \sqrt{\frac{n_e e^2}{\varepsilon_0 m_0}} = \sqrt{\frac{\rho_e}{\varepsilon_0 m_0}}$, $\Omega_n = \omega - \upsilon_0 \beta_n$, $((\gamma_n)^2 = k^2 - (\beta_n)^2)$, A_n^I is the undetermined coefficient; $n = 0, \pm 1, \pm 2, \pm 3, ..., \upsilon = 0, \pm 1, \pm 2, \pm 3, ...$, J_υ and Y_υ is the Bessel function of 1st and 2nd kind of order υ

3.3.2 EM Field Expression for Region-II (i.e., $r_e < r < r_d$)

The two consecutive disks that are separated by axial distance (L − T) show free space in region-II (i.e., disk present free-space region contains standing wave due to the reflections from the metal disk) producing an integral number of half guide wavelengths and can be written as [Tripathi *et al., 2020*- Dwivedi *et al., 2012*- Kumar *et al. 2020*].

The relevant field equations for the slow wave regime in the disk free region for TM mode are follows as: [Tripathi *et al., 2020*- Dwivedi *et al., 2012*- Kumar *et al. 2020*].

$$E_Z^{II} = \sum_{n=-\infty}^{\infty} \left\{ J_0\left(\gamma_n^{II} r\right) A_n^{II} + Y_0\left(\gamma_n^{II} r\right) B_n^{II} \right\} e^{j(\omega t - \beta_n^{II} Z)} \tag{3.20}$$

$$E_r^{II} = \sum_{n=-\infty}^{\infty} \frac{-j\beta_n^{II}}{\gamma_n^{II}} \left\{ J_0'\left(\gamma_n^{II} r\right) A_n^{II} + Y_0'\left(\gamma_n^{II} r\right) B_n^{II} \right\} e^{j(\omega t - \beta_n^{II} Z)} \tag{3.21}$$

$$H_\theta^{II} = \sum_{n=-\infty}^{\infty} \frac{-j\omega\varepsilon_0}{\gamma_n^{II}} \left\{ J_0'\left(\gamma_n^{II} r\right) A_n^{II} + Y_0'\left(\gamma_n^{II} r\right) B_n^{II} \right\} e^{j(\omega t - \beta_n^{II} Z)} \tag{3.22}$$

In the above EM field expressions, $k\,(=\omega/c)$, $k' = \omega\sqrt{\varepsilon_0 \mu_o \varepsilon_r}$, $\gamma_n^{II} = \left(k^2 - \left(\beta_n^{II}\right)^2\right)^{1/2}$ and $\beta_n^{II}\,(=\beta_0 + 2n\pi/L)$ are the free-space propagation constant, the propagation constant in

the presence of dielectric material, the radial propagation constant, and the axial propagation constant, respectively. Here, $n(=0,\pm1,\pm2,\pm3.....)$ depicts the number of the space harmonics present in the region–II, J_0 and Y_0 are the Bessel's function of the first and second kind, respectively. The prime used as superscript (J_0' and Y_0') in the Bessel function shows the first derivative of the Bessel function.

3.3.3 EM Field Expression for Region-III (i.e., $r_d < r < r_{DI}$)

The standing wave created by reflections off the metal disc in region-III of the two successive discs, which are separated by the axial distance (L-T), generates an integral number of half guide wavelengths which is expressed by : [Tripathi *et al., 2020*- Dwivedi *et al., 2012*- Kumar *et al. 2020*].

$$(L-T)=\frac{m\lambda_m^{III}}{2} \qquad (m=1,2,3,.....) \tag{3.23}$$

Here, $m(=1,2,3,.....)$ is stationary-wave modal number and λ_m^{III} is guided wavelength of the stationary wave supported by region III. The relationship between the axial phase propagation constant (β_m^{III}) and the half guide wavelengths (λ_m^{III}) is as follows:

$$\lambda_m^{III}=\frac{2\pi}{\beta_m^{III}} \tag{3.24}$$

Then, using (3.20) and (3.21), the relation of β_m^{III} may be stated as follows:

$$\beta_m^{III}=\frac{m\pi}{(L-T)} \qquad (m=1,2,3,.....) \tag{3.25}$$

The EM field expressions in the region–III, can be expressed

$$E_Z^{III} = \sum_{m=1}^{\infty} \left\{ J_0\left(\gamma_m^{III} r\right) A_m^{III} + Y_0\left(\gamma_m^{III} r\right) B_m^{III} \right\} \times e^{j\omega t} Sin\left(\beta_m^{III} Z\right) \tag{3.26}$$

$$E_r^{III} = \sum_{m=1}^{\infty} \frac{-j\beta_m^{III}}{\gamma_m^{III}} \left\{ J_0'\left(\gamma_m^{III} r\right) A_m^{III} + Y_0'\left(\gamma_m^{III} r\right) B_m^{III} \right\} \times e^{j\omega t} Sin\left(\beta_m^{III} Z\right) \tag{3.27}$$

$$H_\theta^{III} = \sum_{m=1}^{\infty} \frac{-j\omega\varepsilon_0}{\gamma_m^{III}} \left\{ J_0'\left(\gamma_m^{III} r_{DI}\right) A_m^{III} + Y_0'\left(\gamma_m^{III} r_{DI}\right) B_m^{III} \right\} \times e^{j\omega t} Sin\left(\beta_m^{III} Z\right) \tag{3.28}$$

Where, β_m^{III}, $\gamma_m^{III}\left(=\sqrt{\left((k)^2-\beta_m^2\right)}\right)$ and k are the axial propagation constant, radial propagation constant, and free space propagation constant, respectively. A_m^{III} and B_m^{III} are the unknown coefficient. The remaining EM field equations reduced to zero like other region.

3.3.4 EM Field Expression for Region-IV (i.e., $r_{DI} < r < r_W$)

The electric and magnetic field expressions in the dielectric-filled region (i.e., region-IV) with the dielectric constant (ε_r) may be represented as with reference to the m^{th} stationary-wave modal harmonic [Tripathi *et al., 2020*- Dwivedi *et al., 2012*- Kumar *et al. 2020*].

$$E_Z^{IV} = \sum_{m=1}^{\infty} A_m^{IV} X_0\left(\gamma_m^{IV} r\right) \times e^{j\omega t} Sin\left(\beta_m^{IV} Z\right) \tag{3.29}$$

$$E_r^{IV} = \sum_{m=1}^{\infty} \frac{-j\beta_m^{IV}}{\gamma_m^{IV}} A_m^{IV} X_0'\left(\gamma_m^{IV} r\right) \times e^{j\omega t} Sin\left(\beta_m^{IV} Z\right) \tag{3.30}$$

$$H_\theta^{IV} = \sum_{m=1}^{\infty} \frac{-j\omega\varepsilon_0\varepsilon_r}{\gamma_m^{IV}} A_m^{IV} X_0'\left(\gamma_m^{IV} r\right) \times e^{j\omega t} Sin\left(\beta_m^{IV} Z\right) \tag{3.31}$$

Where, $\gamma_m^{IV} = \sqrt{\left((\varepsilon_r k)^2 - \beta_m^2\right)}$ is the radial propagation constant of the region–IV. $X_0\left(\gamma_m^{IV} r\right)$ is the new constant in the above EM field equation and expressed as :

$$X_0\left(\gamma_m^{IV} r\right) = \left\{ J_o\left(\gamma_m^{IV} r\right) Y_o\left(\gamma_m^{IV} r_w\right) - J_o\left(\gamma_m^{IV} r_w\right) Y_o\left(\gamma_m^{IV} r\right) \right\}$$

Where $X_0'\left(\gamma_m^{IV} r\right)$ is the first derivative of the expression $X_0\left(\gamma_m^{IV} r\right)$. The rest of EM field equation is zero similar to other region.

3.4 Boundary Conditions

Here, the three discontinuities exist in the corresponding periodic metal disc-loaded co-axial structure i.e., between region–I and region–II (for $r = r_e$), between region–II and region–III (for $r = r_d$) and between the region–II and the region–III (for $r = r_{Dl}$). The following are the EM boundary conditions for this structure:

The axial electric field intensity at the metallic surface (i.e., $r = r_c$, $0 \le \theta \le 2\pi$), can be expressed as [Tripathi *et al., 2020*- Dwivedi *et al., 2012*- Kumar *et al. 2020*].

$$E_z^I = 0 \qquad 0 \le z < \infty \tag{3.32}$$

(1) The boundary condition between region – I and region – II at $r = r_e$

$$E_Z^{II}(r_e) = E_Z^I(r_e) \tag{3.33}$$

$$H_\theta^I = H_\theta^{II} \tag{3.34}$$

(2) The boundary condition between region – II and region – III at $r = r_d$

$$E_z^{II} = \begin{cases} E_z^{III} & 0 < z < (L-T) \\ 0 & (L-T) \le z \le L \end{cases} \tag{3.35}$$

$$H_\theta^{II} = H_\theta^{III} \qquad 0 < z < (L-T) \tag{3.36}$$

(3) The boundary condition between region – III and region – IV at $r = r_{Dl}$

$$E_z^{III} = E_z^{IV} \qquad 0 < z < (L-T) \tag{3.37}$$

$$H_{\theta}^{III} = H_{\theta}^{IV} \qquad 0 < z < (L-T) \tag{3.38}$$

3.5 Dispersion Relationship

The partially filled periodic metal disc-loaded co-axial structure's dispersion relation was discovered using the field matching approach. A set of simultaneous equations was formed utilizing the aforementioned boundary conditions. These sets of simultaneous equations are built out in the determinant form, that connects the axial phase constant (or phase velocity) and wave frequency.

3.5.1. For Regions-III and –IV

First, the electric field expression of the region-III expressed in equation (3.26), and the electric field expression of the region-IV given in equation (3.29) are substituted into the boundary condition to obtain the dispersion relation for the partially dielectric-filled periodic disc-loaded coaxial waveguide structure (3.37).

$$E_z^{IV} = E_z^{III} \quad \text{at } r = r_{Dl} \tag{3.39}$$

$$\sum_{m=1}^{\infty} A_m^{IV} X_0\left(\gamma_m^{IV} r\right) \times e^{j\omega t} Sin\left(\beta_m^{IV} Z\right) = \sum_{m=1}^{\infty} \left\{ A_m^{III} J_0\left(\gamma_m^{III} r_{Dl}\right) + B_m^{III} J_0\left(\gamma_m^{III} r_{Dl}\right) \right\} \times e^{j\omega t} Sin\left(\beta_m^{III} Z\right) \tag{3.39.1}$$

The time dependency has been excluded from the derivation in this case for the purpose of simplicity. The aforementioned formula may be used to derive the following relationship between field coefficients:

$$A_m^{IV} = A_m^{III} \frac{\left(J_0\left(\gamma_m^{III} r_{Dl}\right)\right)}{\left(X_0\left(\gamma_m^{IV} r_{Dl}\right)\right)} + B_m^{III} \frac{\left(Y_0\left(\gamma_m^{III} r_{Dl}\right)\right)}{\left(X_0\left(\gamma_m^{IV} r_{Dl}\right)\right)} \tag{3.39.2}$$

Similarly apply the boundary conditions for magnetic field:

$$H_\theta^{IV} = H_\theta^{III} \text{ at } r = r_{Dl} \tag{3.40}$$

$$\sum_{m=1}^{\infty} \frac{-j\omega\varepsilon_0\varepsilon_r}{\gamma_m^{IV}} A_m^{IV} X_0{}'\left(\gamma_m^{IV} r\right) \times e^{j\omega t} Sin\left(\beta_m^{IV} Z\right) = \sum_{m=1}^{\infty} \frac{-j\omega\varepsilon_0}{\gamma_m^{III}} \left\{ J_0'\left(\gamma_m^{III} r\right) A_m^{III} + Y_0'\left(\gamma_m^{III} r\right) B_m^{III} \right\} \times e^{j\omega t} Sin\left(\beta_m^{III} Z\right) \tag{3.40.1}$$

$$A_m^{IV} = A_m^{III} \left(\frac{\gamma_m^{III}}{\varepsilon_r \gamma_m^{IV}} \right) \frac{\left(J_0'\left(\gamma_m^{III} r_{Dl}\right)\right)}{\left(X_0'\left(\gamma_m^{IV} r_{Dl}\right)\right)} + B_m^{III} \left(\frac{\gamma_m^{III}}{\varepsilon_r \gamma_m^{IV}} \right) \frac{\left(Y_0'\left(\gamma_m^{III} r_{Dl}\right)\right)}{\left(X_0'\left(\gamma_m^{IV} r_{Dl}\right)\right)} \tag{3.40.2}$$

So,

$$A_m^{III} \left(\frac{\gamma_m^{III}}{\varepsilon_r \gamma_m^{IV}} \right) \frac{\left(J_0'\left(\gamma_m^{III} r_{Dl}\right)\right)}{\left(X_0'\left(\gamma_m^{IV} r_{Dl}\right)\right)} - A_m^{III} \frac{\left(J_0\left(\gamma_m^{III} r_{Dl}\right)\right)}{\left(X_0\left(\gamma_m^{IV} r_{Dl}\right)\right)} = B_m^{III} \frac{\left(Y_0\left(\gamma_m^{III} r_{Dl}\right)\right)}{\left(X_0\left(\gamma_m^{IV} r_{Dl}\right)\right)} - B_m^{III} \left(\frac{\gamma_m^{III}}{\varepsilon_r \gamma_m^{IV}} \right) \frac{\left(Y_0'\left(\gamma_m^{III} r_{Dl}\right)\right)}{\left(X_0'\left(\gamma_m^{IV} r_{Dl}\right)\right)} \tag{3.40.3}$$

Here, a new constant ξ is added as follows to simplify the equations:

$$\frac{\varepsilon_r \gamma_m^{III} X_0'\left(\gamma_m^{IV} r_{Dl}\right) Y_0\left(\gamma_m^{III} r_{Dl}\right) - \gamma_m^{IV} X_0\left(\gamma_m^{IV} r_{Dl}\right) Y_0'\left(\gamma_m^{III} r_{Dl}\right)}{\varepsilon_r \gamma_m^{IV} X_0'\left(\gamma_m^{IV} r_{Dl}\right) X_0\left(\gamma_m^{IV} r_{Dl}\right)} B_m^{III} = \frac{\gamma_m^{IV} X_0\left(\gamma_m^{IV} r_{Dl}\right) J_0'\left(\gamma_m r_{Dl}\right) - \varepsilon_r \gamma_m^{III} X_0'\left(\gamma_m^{IV} r_{Dl}\right) J_0\left(\gamma_m^{III} r_{Dl}\right)}{\varepsilon_r \gamma_m^{IV} X_0'\left(\gamma_m^{IV} r_{Dl}\right) X_0\left(\gamma_m^{IV} r_{Dl}\right)} A_m^{III} = \xi \tag{3.40.4}$$

$$\xi^{III} = \frac{B_m^{III}}{A_m^{III}} = \frac{\gamma_m^{IV} X_0\left(\gamma_m^{IV} r_{Dl}\right) J_0'\left(\gamma_m^{III} r_{Dl}\right) - \varepsilon_r \gamma_m^{III} X_0'\left(\gamma_m^{IV} r_{Dl}\right) J_0\left(\gamma_m^{III} r_{Dl}\right)}{\varepsilon_r \gamma_m^{III} X_0'\left(\gamma_m^{IV} r_{Dl}\right) Y_0\left(\gamma_m^{III} r_{Dl}\right) - \gamma_m^{IV} X_0\left(\gamma_m^{IV} r_{Dl}\right) Y_0'\left(\gamma_m^{III} r_{Dl}\right)} \tag{3.40.5}$$

3.5.2 Boundary Conditions between region –III and region –II

When author apply the boundary conditions for electric field analysis for region III and II

$$E_z^{III} = E_z^{II} \quad \text{at } r = r_d \tag{3.41}$$

$$\sum_{m=1}^{\infty}\left\{J_0\left(\gamma_m^{III} r_d\right) A_m^{III} + Y_0\left(\gamma_m^{III} r_d\right) B_m^{III}\right\} \times e^{j\omega t} Sin\left(\beta_m^{III} Z\right) = \sum_{n=-\infty}^{\infty}\left\{J_0\left(\gamma_n^{II} r_d\right) A_n^{II} + Y_0\left(\gamma_n^{II} r_d\right) B_n^{II}\right\} e^{j(\omega t - \beta_n Z)} \tag{3.41.1}$$

Multiplying both side by $Sin(\beta_m Z)$ and integrate from $0 < Z < L - T$ we obtain the relation among A_m^{III} and A_n^{II} that is

$$\sum_{m=1}^{\infty} A_m^{III}\left\{J_0\left(\gamma_m^{III} r_d\right) + \xi^{III} Y_0\left(\gamma_m^{III} r_d\right)\right\} \int_0^{L-T} \left(Sin\left(\beta_m Z\right)\right)^2 dZ = \sum_{n=-\infty}^{\infty}\left\{J_0\left(\gamma_n^{II} r_d\right) A_n^{II} + Y_0\left(\gamma_n^{II} r_d\right) B_n^{II}\right\} \int_0^{L-T} e^{-j\beta_n Z}\left(Sin\left(\beta_m Z\right)\right) dZ \tag{3.41.2}$$

$$A_m^{III} = \sum_{n=-\infty}^{\infty}\left[\left\{\frac{J_0\left(\gamma_n^{II} r_d\right)}{J_0\left(\gamma_m^{III} r_d\right) + \xi^{III} Y_o\left(\gamma_m^{III} r_d\right)}\right\} A_n^{II} + \left\{\frac{Y_0\left(\gamma_n^{II} r_d\right)}{J_0\left(\gamma_m^{III} r_d\right) + \xi^{III} Y_o\left(\gamma_m^{III} r_d\right)}\right\} B_n^{II}\right] \times \left\{\frac{2\beta_m}{(L-T)\left(\beta_n^2 - \beta_m^2\right)}\left((-1) + (-1)^m e^{-j\beta_n L}\right)\right\} \tag{3.41.3}$$

Similarly for magnetic field analysis

$$H_\theta^{III} = H_\theta^{II} \qquad \text{at } r = r_d \tag{3.42}$$

$$\sum_{m=1}^{\infty} \frac{-j\omega\varepsilon_0}{\gamma_m^{III}}\left\{J_0'\left(\gamma_m^{III} r_d\right) A_m^{III} + \xi^{III} Y_0'\left(\gamma_m^{III} r_d\right) B_m^{III}\right\} \times e^{j\omega t} Sin\left(\beta_m Z\right) = \sum_{n=-\infty}^{\infty} \frac{-j\omega\varepsilon_0}{\gamma_n^{II}}\left\{J_0'\left(\gamma_n^{II} r_d\right) A_n^{II} + Y_0'\left(\gamma_n^{II} r_d\right) B_n^{II}\right\} e^{j(\omega t - \beta_n Z)} \tag{3.42.1}$$

Multiplying both side by $Sin(\beta_m Z)$ and integrate from $0 < Z < L - T$ we obtain the relation among A_m^{III} and A_n^{II} that is

$$A_m^{III} = \sum_{n=-\infty}^{\infty} \left(\frac{\gamma_m^{III}}{\gamma_n^{II}}\right)\left[\left\{\frac{J_0'\left(\gamma_n^{II} r_d\right)}{J_0'\left(\gamma_m^{III} r_d\right) + \xi^{III} Y_0'\left(\gamma_m^{III} r_d\right)}\right\} A_n^{II} + \left\{\frac{Y_0'\left(\gamma_n^{II} r_d\right)}{J_0'\left(\gamma_m^{III} r_d\right) + \xi^{III} Y_0'\left(\gamma_m^{III} r_d\right)}\right\} B_n^{II}\right] \times \left\{\frac{2\beta_m}{(L-T)\left(\beta_n^2 - \beta_m^2\right)}\left((-1) + (-1)^m e^{-j(L-T)\beta_n}\right)\right\} \tag{3.42.2}$$

Thus we get

$$\sum_{n=-\infty}^{\infty}\left[\left\{\frac{J_0\left(\gamma_n^{II}r_d\right)\left(\left(-1\right)+\left(-1\right)^m e^{-j\beta_n L}\right)}{J_0\left(\gamma_m^{III}r_d\right)+\xi^{III}Y_0\left(\gamma_m^{III}r_d\right)}\right\}A_n^{II}-\left(\frac{\gamma_m^{III}}{\gamma_n^{II}}\right)\left\{\frac{J_0'\left(\gamma_n^{II}r_d\right)\left(\left(-1\right)+\left(-1\right)^m e^{-j(L-T)\beta_n}\right)}{J_0'\left(\gamma_m^{III}r_d\right)+\xi^{III}Y_0'\left(\gamma_m^{III}r_d\right)}\right\}A_n^{II}\right]$$
$$=\sum_{n=-\infty}^{\infty}\left[\left(\frac{\gamma_m}{\gamma_n}\right)\left\{\frac{Y_0'\left(\gamma_n^{II}r_d\right)\left(\left(-1\right)+\left(-1\right)^m e^{-j(L-T)\beta_n}\right)}{J_0'\left(\gamma_m^{III}r_d\right)+\xi^{III}Y_0'\left(\gamma_m^{III}r_d\right)}\right\}B_n^{II}-\left\{\frac{Y_0\left(\gamma_n^{II}r_d\right)\left(\left(-1\right)+\left(-1\right)^m e^{-j\beta_n L}\right)}{J_0\left(\gamma_m^{III}r_d\right)+\xi^{III}Y_0\left(\gamma_m^{III}r_d\right)}\right\}B_n^{II}\right] \quad (3.42.3)$$

So,

$$\frac{B_n^{II}}{A_n^{II}}=\frac{\gamma_m^{III}Y_0'\left(\gamma_n^{II}r_d\right)\left(J_0\left(\gamma_m^{III}r_d\right)+\xi^{III}Y_0\left(\gamma_m^{III}r_d\right)\right)\left(\left(-1\right)+\left(-1\right)^m e^{-j(L-T)\beta_n}\right)-\gamma_n^{II}Y_0\left(\gamma_n^{II}r_d\right)\left(J_0'\left(\gamma_m^{III}r_d\right)+\xi^{III}Y_0'\left(\gamma_m^{III}r_d\right)\right)\left(\left(-1\right)+\left(-1\right)^m e^{-j\beta_n L}\right)}{\gamma_n^{II}J_0\left(\gamma_n^{II}r_d\right)\left(J_0'\left(\gamma_m^{III}r_d\right)+\xi^{III}Y_0'\left(\gamma_m^{III}r_d\right)\right)\left(\left(-1\right)+\left(-1\right)^m e^{-j\beta_n L}\right)-\gamma_n J_0'\left(\gamma_n^{II}r_d\right)\left(J_0\left(\gamma_m^{III}r_d\right)+\xi^{III}Y_0\left(\gamma_m^{III}r_d\right)\right)\left(\left(-1\right)+\left(-1\right)^m e^{-j(L-T)\beta_n}\right)} \quad (3.42.4)$$

$$\frac{B_n^{II}}{A_n^{II}}=\xi^{II} \quad (3.42.5)$$

$$\xi^{II}=\frac{\gamma_m^{III}Y_0'\left(\gamma_n^{II}r_d\right)\left(J_0\left(\gamma_m^{III}r_d\right)+\xi^{III}Y_0\left(\gamma_m^{III}r_d\right)\right)\left(\left(-1\right)+\left(-1\right)^m e^{-j(L-T)\beta_n}\right)-\gamma_n^{II}Y_0\left(\gamma_n^{II}r_d\right)\left(J_0'\left(\gamma_m^{III}r_d\right)+\xi^{III}Y_0'\left(\gamma_m^{III}r_d\right)\right)\left(\left(-1\right)+\left(-1\right)^m e^{-j\beta_n L}\right)}{\gamma_n^{II}J_0\left(\gamma_n^{II}r_d\right)\left(J_0'\left(\gamma_m^{III}r_d\right)+\xi^{III}Y_0'\left(\gamma_m^{III}r_d\right)\right)\left(\left(-1\right)+\left(-1\right)^m e^{-j\beta_n L}\right)-\gamma_n J_0'\left(\gamma_n^{II}r_d\right)\left(J_0\left(\gamma_m^{III}r_d\right)+\xi^{III}Y_0\left(\gamma_m^{III}r_d\right)\right)\left(\left(-1\right)+\left(-1\right)^m e^{-j(L-T)\beta_n}\right)} \quad (3.42.6)$$

3.5.3 Boundary condition between region I and region II

The relationship between unknowns appears similarly in regions II and I.

$$E_Z^{II}\left(r_e\right)=E_Z^{I}\left(r_e\right) \quad (3.43)$$

$$\frac{dE_Z^{II}\left(r_e\right)}{dr}-\frac{dE_Z^{I}\left(r_e\right)}{dr}=\frac{2\alpha}{\pi r_e}\frac{\gamma_n^2C^2}{\Omega_n^2}E_Z^{I}\left(r_e\right) \quad (3.44)$$

$$A_n^{II}J_0'\left(\gamma_n^{II}r_e\right)+B_n^{II}Y_0'\left(\gamma_n^{II}r_e\right)=G_{2,n}J_0'\left(G_{2,n}r_e\right) \quad (3.45)$$

$$A_n^{II}=\left[Y_0\left(\gamma_n^{I}r_e\right)-\alpha\frac{\left(\gamma_n^{I}\right)^2C^2}{\Omega_n^2}Y_0\left(\gamma_n^{I}r_e\right)\left\{Y_0\left(\gamma_n^{I}r_c\right)J_0\left(\gamma_n^{I}r_e\right)-J_0\left(\gamma_n^{I}r_c\right)Y_0\left(\gamma_n^{I}r_e\right)\right\}\right]A_n^{I} \quad (3.46)$$

$$B_n^{II} = \left[-J_0\left(\gamma_n^I r_c\right) + \alpha \frac{\left(\gamma_n^I\right)^2 C^2}{\Omega_n^2} J_0\left(\gamma_n^I r_c\right)\left\{ Y_0\left(\gamma_n^I r_c\right) J_0\left(\gamma_n^I r_e\right) - J_0\left(\gamma_n^I r_c\right) Y_0\left(\gamma_n^I r_e\right)\right\} \right] A_n^I = \xi^{II} A_n^{II} \quad (3.46.1)$$

Thus, the expression may be rewritten as:

$$A_n^{II} = \sum_{n=-\infty}^{\infty} A_n^I \, S_{n,m} \quad (3.47)$$

Where $S_{n,m}$ and $U_{n,m}$ expressed as:

$$S_{n,m} = \left[Y_0\left(\gamma_n^I r_e\right) - \alpha \frac{\left(\gamma_n^I\right)^2 C^2}{\Omega_n^2} Y_0\left(\gamma_n^I r_e\right)\left\{ Y_0\left(\gamma_n^I r_c\right) J_0\left(\gamma_n^I r_e\right) - J_0\left(\gamma_n^I r_c\right) Y_0\left(\gamma_n^I r_e\right)\right\} \right] A_n^I \quad (3.47.1)$$

$$A_n^{II} = \sum_{n=-\infty}^{\infty} U_{n,m} A_n^I \quad (3.48)$$

$$U_{n,m} = \frac{1}{\xi^{II}} \left[-J_0\left(\gamma_n^I r_c\right) + \alpha \frac{\left(\gamma_n^I\right)^2 C^2}{\Omega_n^2} J_0\left(\gamma_n^I r_c\right)\left\{ Y_0\left(\gamma_n^I r_c\right) J_0\left(\gamma_n^I r_e\right) - J_0\left(\gamma_n^I r_c\right) Y_0\left(\gamma_n^I r_e\right)\right\} \right] \quad (3.48.1)$$

Now, as the expression is given in (3.47) and (3.48) both represented A_n^{II} in the form of the region–I constant A_n^I, thus after equating both the expression and doing some needful derivation we obtained the following expression:

$$\sum_{n=-\infty}^{\infty} \left(S_{n,m} - U_{n,m} \right) A_n^I = 0 \quad (3.49)$$

The above expression (3.49) is formed *m* number of simultaneous series equations of the EM field constant A_n^I where A_n^I itself is of an infinite number $(-\infty < n < \infty)$. One can utilize the determinant approach to solve these simultaneous equations for a nontrivial solution. To find the dispersion relation of the structure, the determinant of the order

$m \times n$ is formed which is set to zero. The final dispersion relation can be calculated as:

$$det\left|S_{n,m} - U_{n,m}\right| = 0 \quad (-\infty < n < \infty,\ 1 \le m < \infty) \tag{3.50}$$

The expression (3.50) depicts set of an infinite number of space harmonics and also stationary wave modes. Here '*det*' is the abbreviation of the determinant. The determinant that is given above has an infinite number of co-efficient which should be truncated up to some level (i.e., some finite order) for solving the above dispersion relation given in expression (3.50).

3.6 Temporal Growth Rate

Only real roots for the eign modes are provided by the dispersion relation when there is no electron beam. The roots of the dispersion relation produce complex roots of frequency for a variety of wave numbers when an electron beam is present. Equation (3.50) is differentiated with respect to ω so as to obtain the temporal growth rate. Between the beam-line cutting point (which is defined as $\omega = \beta_o v_e$) and the slow space charge wave (slow SCW) line on the dispersion curve, this range of wave number is typically known as instability region [Dwivedi *et al.,*2012], [Singh *et al.,* 2004]. The v_e is maximum electron velocity, where, $\omega = \beta_o v_e$ defines the beam-line. The slow SCW is defined by [Singh *et al.,* 2004], $\omega = \beta_o v_{slow-sc}$, here, $v_{slow-sc} = v_e(1 - \omega_p / (\omega_c \gamma^{1.5}{}_o))$. Slow SCW interrelates with the structure-supported RF wave inside of the instability region to create real and imaginary roots of frequency. The oscillation frequency of an RF wave is obtained using the real root of frequency (i.e., f_r), whereas the temporal growth rate is found out with the help of an imaginary root of frequency (i.e., f_i) (i.e., the rate at which the oscillation frequency thrives with time in the instability region). With increase of time,

this imaginary frequency causes RF to exponentially rise (i.e., $e^{-i2\pi(f_r+f_i)t}$) [Dwivedi *et al.,* 2013].

3.7 Results and discussion

The linearized Vlasov-Maxwell's equation has been utilized for the investigation of the beam-wave interaction process in partially dielectric filled MILO, which uses a disc-loaded coaxial waveguide as its RF interaction structure. By the use of field matching, approach beam present analysis for dispersion relation has been obtained for the TM_{00} mode. Quantitative measurements of the intensity of RF radiation are evaluated using the temporal growth rate that is explained by the imaginary value of frequency corresponding to the conjugate roots of the dispersion relation.

If the beam current and energy meet the first threshold for the emergence of instability in the current beam case, the microwave radiation occurs. The dispersion relation (3.50) for a classical structure and beam parameters is numerically calculated to examine the MILO oscillation. For verification of the analysis, the structure has been devised according to the reported design data for the L-band MILO in the literature [Dwivedi *et. al.,* 2013]. The unit structure is used in this simulation because, according to Floquet's theorem, a single unit of a periodic structure is adequate for analysis. Figure 3.2 displays the dispersion curve as determined by the numerical analysis using the EM simulation tool. The beam present dispersion curve generated from numerical analysis and EM tools with the presence and absence of the dielectric loading are in good agreement, as can be seen in figure 3.2. The curve shows the good agreement between simulation and analytical analysis with relative error less than 5%.

The dispersion curve plot shows the effect of dielectric material on the structure.

It clearly shows the operating frequency of the device goes down in the presence of dielectric material.

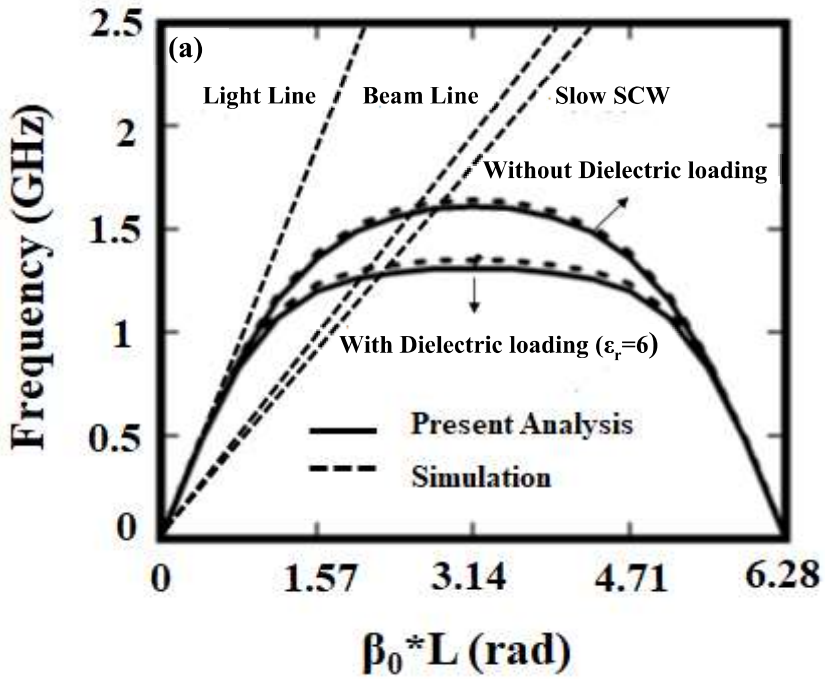

Figure 3.2: Dispersion curve for azimuthally symmetric axially periodic metal disc loaded coaxial partially filled dielectric structure in beam presence at voltage V=420 kV, current I_a=38 kA, (with, r_c=29 mm, r_d=43 mm, r_w= 87 mm, L=20 mm and T=3 mm).

The structure is regarded as a slow wave structure since the dispersion curve is under the light line. The Region between the slow SCW line and the beam line is referred to as the instability region, and it is in this region that the temporal growth rate is obtained. The temporal growth rate (f_i) at distinct phase ($\beta_o \times L$) in radian for different modes as shown in Figure 3.3. The progress of the imaginary part of the frequency (i.e., f_i) with respect to time gives the device a temporal growth rate. Form figure 3.3, the temporal growth rate with dielectric loading is ~0.068 per ns and without dielectric loading is ~0.052 per ns for TM_{00} mode. As the result, growth of RF is high in the presence of

dielectric as compared with without dielectric loading.

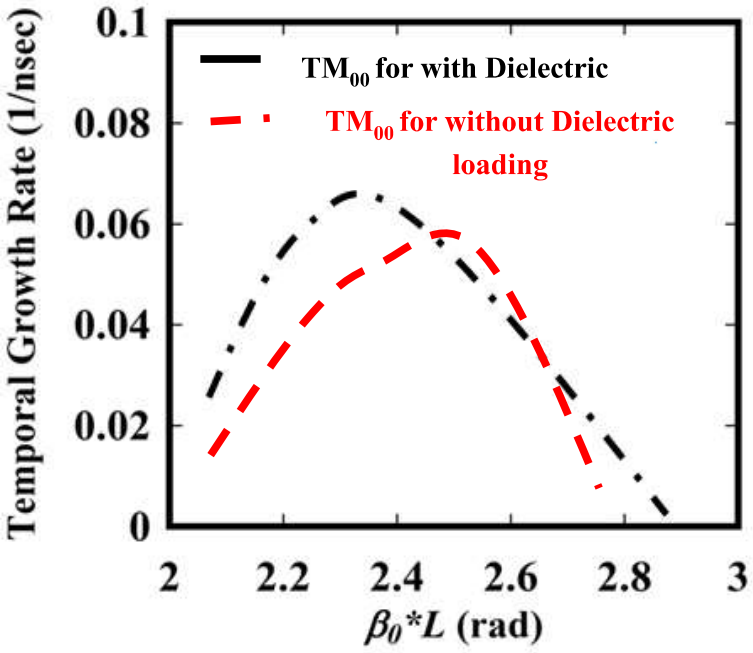

Figure 3.3: Temporal growth rate (f_i) at different phase ($\beta_o \times L$) in radian for two conditions supported by the structure (i.e., in presence of dielectric and without dielectric).

3.8 Conclusion

The azimuthally symmetric axial periodic metal disc loaded coaxial partially dielectric filled structure was examined in this article on the electron beam presence. For the analysis, a field matching approach has been used. The linearized maxwell's fluid equation (i.e., Vlasov-Maxwell's equation) has been utilized for analysis of the region where the electron beam was present (i.e. Region I). The beam-wave interaction investigation of the device primarily aims to find the dispersion relation (in electron beam presence) and temporal growth rate. The dispersion curve, the

temporal growth rate and other parameters are obtained through analytical and simulation analysis, considering all the harmonics developed in the structure. The influence of dielectric material on device parameters has been already investigated in the beam absent analysis. The purpose of this study was to improve the theoretical knowledge of the partially dielectric filled MILO during electron beam present, that may be useful for design engineers working on HPM devices MILO.